Polyelectrolyte based hole-transporting materials for high performance solution processed planar perovskite solar cells†

Xiaodong Li, Xiaohui Liu, Xueyan Wang, Lixiao Zhao, Tonggang Jiu and Junfeng Fang*

Using polyelectrolytes (P3CT-Na) as hole-transporting materials (HTMs), high performance inverted perovskite solar cells with a PCE of 16.6% could be obtained, which was more than 20% improvement compared with those based on the PEDOT:PSS HTM (PCE of 13.7%). The performance improvement can be ascribed to the desirable match of energy levels as well as the better crystalline properties and larger grain size of $CH_3NH_3PbCl_{3-x}I_x$ films on P3CT-Na. Importantly, rather good performance with PCE over 11% is achievable even if the P3CT-Na thickness ranges from 1 nm to 52 nm. Our work indicated the promising applications of polyelectrolyte based HTMs in perovskite solar cells and may provide some insights into the design and synthesis of new HTMs to further improve the device performance.

Perovskite solar cells based on hybrid methylammonium lead halide ($CH_3NH_3PbX_3$, X = halogen) have been intensively studied and considered to be one of the most promising thin film photovoltaic devices for the next generation.[1–3] $CH_3NH_3PbX_3$ perovskite materials exhibited excellent properties for photovoltaic applications, such as broad optical absorbance, low-temperature solution processability, ambipolar transport properties[4] and long electron–hole diffusion length[5,6] (100 nm for triiodide and 1 μm for mixed trihalide perovskite). Initially, Miyasaka and co-workers introduced $CH_3NH_3PbX_3$ into liquid dye-sensitized solar cells (DSSCs) as a sensitizer and a power conversion efficiency (PCE) of 3.8% was obtained.[7] The relative low efficiency was mainly due to the easy dissolution of $CH_3NH_3PbX_3$ in the liquid electrolyte (iodine/iodide redox couple). By replacing the liquid electrolyte with a solid hole-transporting material (HTM), like 2,2′7,7′-tetrakis(*N*,*N*-di-*p*-methoxyphenylamine)-9,9′-spirobifluorene (spiro-MeOTAD), a PCE of >10% and even 17–19% could be obtained by Snaith, Grätzel and Y. Yang *et al.* through morphology control, chemical management and interfacial optimization.[8–19] Generally, these devices used compact or mesoporous TiO_2 as an electron transporting material (ETM) and spiro-MeOTAD as the HTM. However, the high temperature sintering of the TiO_2 ETM as well as the oxidation doping of the spiro-MeOTAD HTM made the device fabrication time-consuming and may also affect the device repeatability.

Alternatively, a so-called inverted p-PSC based on the ITO/PEDOT:PSS substrate was introduced by Jun-Yuan Jeng *et al.* although only a PCE of 3.9% was obtained.[20] Soon, the PCE was increased to 9.8% on the FTO/PEDOT:PSS substrate.[21] Recently, more efficient inverted p-PSCs with PCE >10% have been reported[22–26] and a PCE of ~15% has also been realized through vacuum deposition[27] or two-step fabrication.[22,28–30] In these inverted p-PSCs, the perovskite absorber was sandwiched between the PEDOT:PSS HTM and an electron transport layer (C_{60} or [6,6]-phenyl-C_{61}-butyric acid methyl ester, $PC_{61}BM$), forming a P–I–N junction. Xing *et al.* proved that the time and efficiency of electron transport from $CH_3NH_3PbI_3$ to $PC_{61}BM$ were 0.4 ns and 92%, respectively, indicating efficient electron transport between perovskite and $PC_{61}BM$.[6] However, for hole transport, the three-dimensional inhomogeneities and anisotropic conductivity of PEDOT:PSS due to its lamellar structure may limit the effective collection of carriers.[31,32] In addition, previous reports have proved that the work function (WF) of PEDOT:PSS (4.9–5.1 eV) was usually lower than the ionization potential of perovskite (*e.g.*, 5.3–5.4 eV for $CH_3NH_3PbX_3$).[33] This energy level difference would lead to energy loss at the $CH_3NH_3PbX_3$/PEDOT:PSS interface, thus decreasing the built-in potential and corresponding performance of solar cells.[33] To overcome these disadvantages, several new types of HTMs were developed to replace PEDOT:PSS, such as metal oxides,[34–36] graphene oxide[37] and even the doping of PEDOT:PSS.[33] However, the ultimate device performance was not so ideal due to various potential reasons, such as poor wetting, high-temperature or high-vacuum processes and so on.[34,35]

To further increase the efficiency of low-temperature solution processed inverted p-PSCs, developing some innovative

Institute of New Energy Technology, Ningbo Institute of Materials Technology and Engineering, Chinese Academy of Sciences, Ningbo, 315201, China. E-mail: fangjf@nimte.ac.cn

types of HTMs to replace PEDOT:PSS is necessary. Water soluble polyelectrolytes have been widely utilized in organic light-emitting diodes (OLEDs) and organic solar cells (OSCs) due to their low temperature treatment and solution processability. Through introducing these polyelectrolytes, a dipole could be formed at the interface, thus regulating the WF of the ITO electrode and improving the carrier extraction. However, in perovskite solar cells, the application of polyelectrolytes was rarely reported and the corresponding reason was not clear yet.

In this work, by introducing a water soluble polyelectrolyte, poly[3-(4-carboxylatebutyl)thiophene (P3CT-Na, Fig. 1a), as the HTM, solution processed $CH_3NH_3PbCl_{3-x}I_x$ perovskite as the absorber and $PC_{61}BM/C_{60}$ as the electron transport layer (Fig. 1a), high performance inverted p-PSCs with a PCE of 16.6% (average 15.4%) could be obtained, which was more than 20% improvement compared with those of PEDOT:PSS based devices fabricated under the same conditions (highest PCE of 13.7%, average 11.6%). More importantly, in contrast with most of the polyelectrolytes previously reported in OLED or OSCs, high performance PSCs without any S-shaped *J–V* curves would be achieved even with a thick P3CT-Na layer: PCE over 11% could be obtained with the P3CT-Na thickness ranging from 1 nm to 52 nm. These results indicate the promising applications of water soluble polyelectrolyte based HTMs in inverted perovskite solar cells and may open up some new insights into the design and synthesis of polyelectrolyte based HTMs to further improve the device performance.

Fig. 1b shows the energy level diagram of p-PSCs used in our work. For bare ITO glass, the WF value was 4.85 eV, which was not high enough for efficient hole collection. When PEDOT:PSS was coated on ITO glass, the WF increased to 5.11 eV (Fig. S1†), facilitating the hole collection to some extent. However, the WF was still a little lower compared with the valence band (VB) of $CH_3NH_3PbCl_{3-x}I_x$ (5.3 eV), which may lead to potential energy loss at the $CH_3NH_3PbCl_{3-x}I_x$/PEDOT:PSS interface and decrease the built-in potential of solar cells.[33] To decrease the interfacial energy loss as possible, further increasing the WF of ITO glass was necessary. After introducing P3CT-Na to replace PEDOT:PSS, the ITO WF increased to 5.26 eV, which was 0.15 eV higher than that of PEDOT:PSS and very close to the VB of $CH_3NH_3PbCl_{3-x}I_x$ (5.3 eV). In addition, previous studies on polymer light-emitting diodes (PLEDs) have proved that the maximum current efficiency of PLEDs could be doubled if an electron blocking layer was inserted between PEDOT:PSS and the emissive layer, indicating that PEDOT:PSS did not possess good electron blocking capacity.[38,39] The inability of PEDOT:PSS in blocking electrons may induce severe interfacial recombination, which would limit the performance of p-PSCs with the PEDOT:PSS HTM. And Bolink *et al.* have also found that the performance of p-PSCs could be effectively enhanced by inserting an extra organic layer (polyTPD) between ITO/PEDOT:PSS and the perovskite absorber to block electrons.[40,41] For the P3CT-Na HTM, the lowest unoccupied molecular orbital (LUMO, 3.33 eV) was 0.42 eV closer to vacuum compared with the conduction band (CB) of the $CH_3NH_3PbCl_{3-x}I_x$ absorber (3.75 eV), which was large enough to block the electron transport to the anode, thus inhibiting the potential interfacial recombination and increasing the V_{oc} of devices. In addition, good cathode contact would also be formed as shown in Fig. 1b. As a result, the desirable energy level match between $CH_3NH_3PbCl_{3-x}I_x$ and P3CT-Na or C_{60}/Al as well as the efficient electron blocking capacity made P3CT-Na a good candidate as the HTM for high performance planar perovskite solar cells.

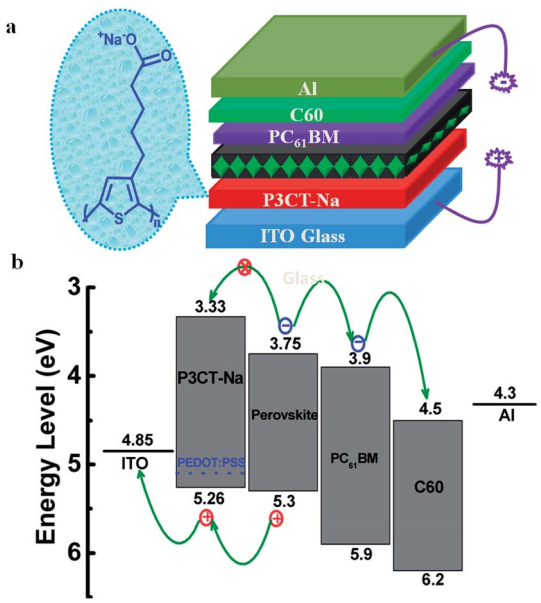

Fig. 1 (a) Chemical structure of P3CT-Na and the device configuration used in our work. (b) The corresponding energy level diagram of perovskite solar cells.

Fig. 2a shows the *J–V* curves of the best inverted p-PSCs with P3CT-Na and PEDOT:PSS under AM 1.5 (100 mW cm^{-2}) illumination. For the PEDOT:PSS based devices, a moderate PCE of 13.7% (average 11.6%) was obtained, mainly due to the inferior V_{oc} of 0.92 V and FF of 65% despite the high J_{sc} of 22.85 mA cm^{-2}. Remarkably, through introducing P3CT-Na to replace PEDOT:PSS, the best PCE rockets to 16.6%, which was 21% improvement compared with those of PEDOT:PSS based devices. The improvement was mainly due to the impressive increase in V_{oc} (from 0.92 V to 1.07 V) and FF (from 65% to 73%), although the J_{sc} slightly decreased to 21.14 mA cm^{-2}, which may be caused by the decreased light transmittance of P3CT-Na coated ITO (Fig. S2†). In solar cells, the V_{oc} was determined by the build-in potential (V_{bi}). To compare the V_{bi} of p-PSCs on P3CT-Na and PEDOT:PSS, the relationship between the net photocurrent density (ΔJ, the difference of photocurrent between under illumination and under dark conditions) and applied voltage is shown in the inset of Fig. 2a.[33] According to eqn (1), the V_{bi} was correlated with the compensation voltage V_0 at which $\Delta J = 0$:

$$V_0 = V_{bi} - \frac{K_B T}{e} \ln(A) \quad (1)$$

where K_B, T, e and A are the Boltzmann constant, absolute temperature, the magnitude of the electron charge and a material parameter, respectively. The higher V_0 for p-PSCs on

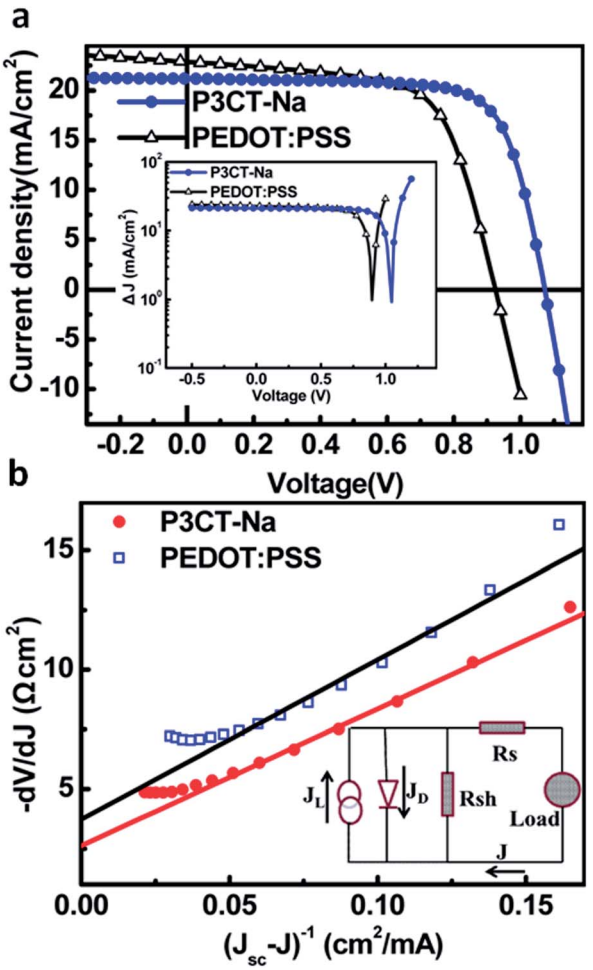

Fig. 2 (a) J–V curves of the best p-PSCs with PEDOT:PSS and the P3CT-Na layer, inset: the difference of photocurrent between under illumination and in the dark (ΔJ) *vs.* voltage applied on p-PSCs; (b) plots of $-\mathrm{d}V/\mathrm{d}J$ *vs.* $(J_{sc} - J)^{-1}$ and the linear fitting curves, inset: the equivalent circuit for p-PSCs with J_L (light-induced constant current), J_D (current of the PN junction diode), R_s (series resistance), R_{sh} (shunt resistance), and J (current flowing through the external load).

P3CT-Na (1.05 V, V_0 of p-PSCs on PEDOT:PSS was 0.89 V) meant the increased forward diffusion of carriers in $CH_3NH_3PbCl_{3-x}I_x$, which would lead to a larger V_{bi}, agreeing with the improved V_{oc} for p-PSCs on P3CT-Na.[33] As to the FF, it was correlated with the series resistance (R_s) of solar cells. According to the equivalent circuit of solar cells in the inset of Fig. 2b (J_L is the light-induced constant current density and J_D is the current density of the PN junction diode),[42] eqn (2) could be deduced (considering the shunt resistance, R_{sh} was very large):

$$-\frac{\mathrm{d}V}{\mathrm{d}J} = \frac{AK_BT}{e}(J_{sc} - J)^{-1} + R_s \qquad (2)$$

Fig. 2b shows the plots of $-\mathrm{d}V/\mathrm{d}J$ *vs.* $(J_{sc} - J)^{-1}$ and linear fitting curves of eqn (2). The good linear relation between $-\mathrm{d}V/\mathrm{d}J$ and $(J_{sc} - J)^{-1}$ means that both the p-PSCs based on P3CT-Na and PEDOT:PSS were well-behaved heterojunction solar cells to some extent.[43] And the intercept of linear fitting curves meant the magnitude of R_s in solar cells. Obviously, the p-PSCs on P3CT-Na exhibited a R_s of 2.18 Ωcm^2, which was about 48% smaller than that of p-PSCs on PEDOT:PSS (R_s of 3.22 Ωcm^2). The relatively small R_s of p-PSCs on P3CT-Na would lead to the improved FF of solar cells, in agreement with that shown in Fig. 2a. Furthermore, the J–V hysteresis is a hot topic in some perovskite solar cells,[44–48] but no obvious hysteresis was observed in our devices with the P3CT-Na HTM (Fig. S3†). And the statistical analysis of the device performance with P3CT-Na and PEDOT:PSS is shown in Fig. S4.†

Fig. 3a and b show the scanning electron microscopy (SEM) images of $CH_3NH_3PbCl_{3-x}I_x$ deposited on P3CT-Na and PEDOT:PSS, respectively. The perovskite films on P3CT-Na exhibited larger grain size and lower number of pinholes than those on PEDOT:PSS, which would lead to much lower grain boundary density. X-ray photoelectron and thermal admittance spectroscopy in previous studies have proved that the trap states induced by the grain boundary could introduce sub-gap states in perovskite films and reduce the device V_{oc} and FF due to the hole accumulation caused by the trap filling of photo-generated electrons.[49,50] And the lower number of pinholes in $CH_3NH_3PbCl_{3-x}I_x$ on P3CT-Na would also prevent the potential contact of P3CT-Na and PCBM, thus inhibiting the leakage current and further improving the V_{oc} and FF as well as the device performance. Fig. 3c shows the X-ray diffraction (XRD) patterns of $CH_3NH_3PbCl_{3-x}I_x$ grown on P3CT-Na and PEDOT:PSS. The peaks at 14.5°, 28.7°, 43.6° and 59.2° could be attributed to the (110), (220), (330) and (440) faces of the tetragonal $CH_3NH_3PbCl_{3-x}I_x$ crystal structure, which was similar to previous studies.[51] Note that all the XRD peaks were impressively enhanced when using P3CT-Na to replace PEDOT:PSS as the HTM, indicating the much improved crystalline properties of perovskite films on P3CT-Na.[51] In addition, the full width at half maximum (FWHM) of the (110) peak for perovskite films on P3CT-Na was much narrower than that on

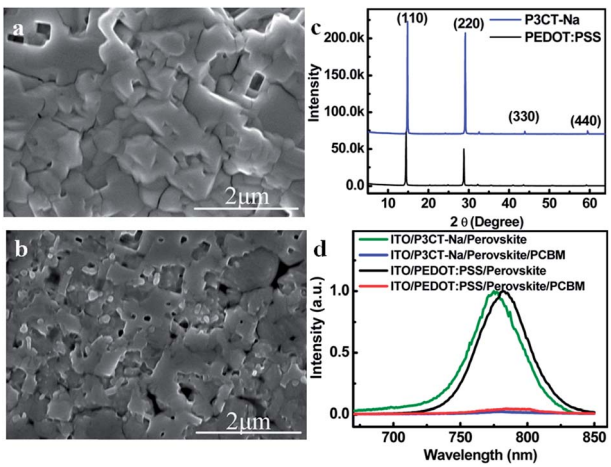

Fig. 3 (a) SEM images of $CH_3NH_3PbCl_{3-x}I_x$ films deposited on ITO/P3CT-Na and (b) ITO/PEDOT:PSS; (c) XRD of $CH_3NH_3PbCl_{3-x}I_x$ films on ITO/P3CT-Na and ITO/PEDOT:PSS; (d) steady state photoluminescence (ST-PL) of $CH_3NH_3PbCl_{3-x}I_x$ films and ITO/P3CT-Na and ITO/PEDOT:PSS.

PEDOT:PSS, which also showed the better crystalline properties for perovskite on P3CT-Na.

Fig. 3d shows steady state photoluminescence (ST-PL) spectra (excited at 600 nm) of $CH_3NH_3PbCl_{3-x}I_x$ deposited on P3CT-Na and PEDOT:PSS, respectively. When PCBM was spin-coated on $CH_3NH_3PbCl_{3-x}I_x$ films, the ST-PL of $CH_3NH_3PbCl_{3-x}I_x$ could be quenched due to the efficient carrier separation between $CH_3NH_3PbCl_{3-x}I_x$ and PCBM. For $CH_3NH_3PbCl_{3-x}I_x$ on P3CT-Na, 97.9% ST-PL would be quenched, while only 95.5% ST-PL quenched for that on PEDOT:PSS, indicating more efficient carrier separation and transport when $CH_3NH_3PbCl_{3-x}I_x$ was deposited on P3CT-Na. Notably, the PL emission peak of $CH_3NH_3PbCl_{3-x}I_x$ on P3CT-Na appeared at 775 nm, while $CH_3NH_3PbCl_{3-x}I_x$ on PEDOT:PSS exhibited an emission peak at 782 nm, which was about 7 nm red shifted compared with that on P3CT-Na. The red shift in the emission peak may be caused by the relaxation of photoexcitons to low energy excited states due to the presence of sub-gap states induced by the crystal grain boundary in $CH_3NH_3PbCl_{3-x}I_x$ deposited on PEDOT:PSS.[52,53] In addition, the time-resolved PL decay also showed that $CH_3NH_3PbCl_{3-x}I_x$ on P3CT-Na exhibited a much longer decay time than that on PEDOT:PSS, indicating longer exciton diffusion lengths and reduced recombination, which also proved the lower number of traps or sub-gap states in $CH_3NH_3PbCl_{3-x}I_x$ on P3CT-Na to some extent (Fig. S5†).[52]

All the studies mentioned above showed the excellent function of the water soluble polyelectrolyte P3CT-Na as a HTM in inverted p-PSCs. In OLEDs or OSCs, the device performance strongly depended on the film thickness of the polyelectrolyte interlayer: the interlayer thickness must be well controlled and generally >10 nm interlayers would cause S-shaped *J–V* curves, strongly decreasing the performance of devices.[54,55] However, for P3CT-Na, all devices showed average PCE over 11% even though the thickness of P3CT-Na ranged from 1 nm to 52 nm. And a PCE of 9% without any S-shaped *J–V* curves could still be obtained even with an 80 nm P3CT-Na layer. Table 1 and Fig. 4a show the specific photovoltaic parameters. When 1 nm P3CT-Na was introduced, an average PCE of 12.3% (highest 12.8%) could be obtained with a V_{oc} of 0.93 V, a J_{sc} of 19.67 mA cm^{-2} and a FF of 67%. If the thickness was increased to 4 nm, much higher V_{oc} (1.05 V) and FF (74%) were obtained, leading to the peak device performance with a PCE of 15.4% (highest 16.6%). Further increasing the thickness of P3CT-Na, the PCE started to decrease mainly due to the decreased J_{sc}. For example, when the P3CT-Na thickness was 27, 52, and 80 nm, the corresponding J_{sc} values were 18.93, 15.21 and 13.52 mA cm^{-2}, respectively. Importantly, even though the thickness of P3CT-Na widely ranged from 1 nm to 80 nm, high V_{oc} (>0.9 V) and FF (~70%) could be obtained, indicating the excellent hole transport properties of P3CT-Na. In addition, scanning electron microscopy (SEM) and atomic force microscopy (AFM) were conducted to study the film morphology of P3CT-Na (Fig. S6 and S7†). The appearance of bright particles indicated that P3CT-Na would aggregate together on ITO glass and form some column-like structure, leading to coarser films. These column-like structures may act as scaffolds for perovskite absorbers to grow on and could also extend into the bulk of the $CH_3NH_3PbCl_{3-x}I_x$ layer to benefit the carrier collection, which may be a reasonable explanation for the good device performance even with a thick P3CT-Na layer (like 52 nm).

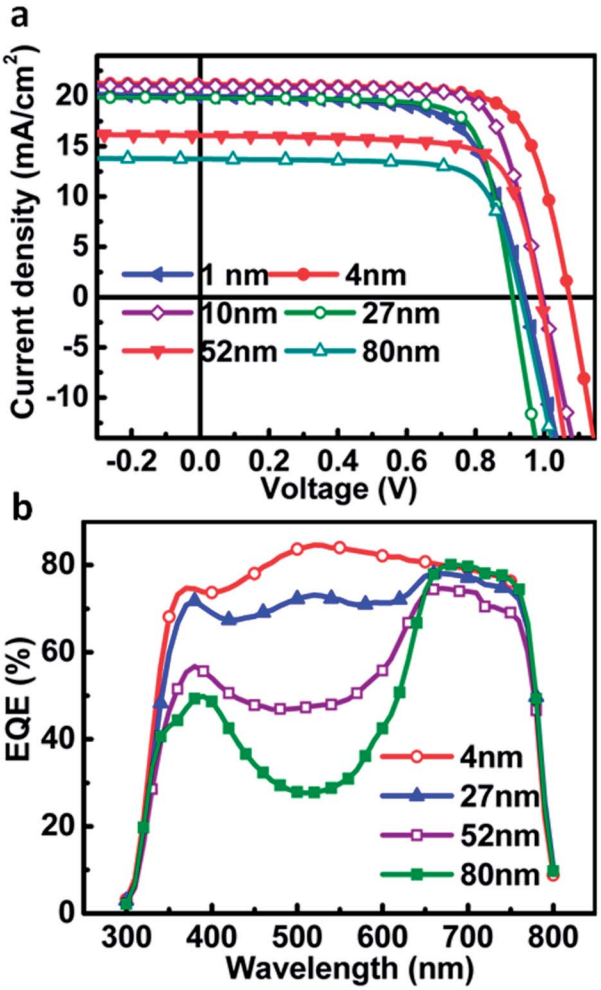

Fig. 4 (a) *J–V* curves and (b) EQE of p-PSCs with different thicknesses of the P3CT-Na layer.

Table 1 The photovoltaic parameters of devices with PEDOT:PSS or different P3CT-Na thicknesses under AM 1.5 (100 mW cm^{-2}) illumination

Thickness[a] (nm)	V_{oc} (V)	J_{sc} (mA cm^{-2})	FF (%)	PCE[b] (%)
1	0.94 (0.93)	19.98 (19.67)	68 (67)	12.8 (12.3)
4	1.07 (1.05)	21.14 (19.93)	73 (74)	16.6 (15.4)
10	0.99 (0.98)	20.98 (20.25)	75 (73)	15.6 (14.5)
27	0.91 (0.93)	19.83 (18.93)	75 (70)	13.6 (12.7)
52	0.99 (0.98)	16.07 (15.21)	74 (74)	11.8 (11.0)
80	0.93 (0.92)	13.73 (13.52)	75 (72)	9.5 (9.0)
PEDOT:PSS	0.92 (0.89)	22.85 (21.20)	65 (62)	13.7 (11.6)

[a] The thickness of the P3CT-Na layer. [b] The values in brackets are average values. The average PCE of devices with 4 nm P3CT-Na and PEDOT:PSS was among 15 separated devices and others were among 6 devices.

To understand the decreased J_{sc} for devices with increasing P3CT-Na thickness, we measured the external quantum efficiency (EQE) of devices with different P3CT-Na thicknesses (Fig. 4b). For devices with 4 nm P3CT-Na, a high EQE value of ~80% could be obtained in the wavelength range of 400 nm to 750 nm and the fitting J_{sc} (20.74 mA cm^{-2}) agreed well with that obtained from J–V curves (21.14 mA cm^{-2}). With the increase of P3CT-Na thickness (from 4 nm to 27, 52 and 80 nm), an EQE valley appeared in the wavelength range of 400 nm to 650 nm and even an EQE <30% (at ~540 nm) was observed for the device with 80 nm P3CT-Na. However, the EQE value in the wavelength range of 650 nm to 750 nm was always stabilized at ~80% no matter how thick the P3CT-Na layer was. Considering the UV-visible absorbance spectroscopy of P3CT-Na (Fig. S8,† the P3CT-Na films showed strong absorbance from 400 nm to 650 nm), the decrease of EQE as well as the corresponding J_{sc} could be ascribed to the absorbance of the P3CT-Na layer.

Conclusions

In conclusion, a water soluble polyelectrolyte (P3CT-Na) was successfully introduced into perovskite solar cells as the HTM and a PCE of 16.6% could be obtained. The P3CT-Na HTM could effectively transport holes and block electrons to the anode, limiting the potential interfacial recombination and increasing the V_{oc} and FF of devices. XRD, SEM and PL spectral measurements showed that $CH_3NH_3PbCl_{3-x}I_x$ on P3CT-Na exhibited better crystalline properties, larger grain size, lower number of pinholes as well as better PL quenching efficiency with PCBM, which would greatly reduce the traps or sub-gap states in $CH_3NH_3PbCl_{3-x}I_x$, thus improving the device performance. In addition, the devices based on P3CT-Na would always show good performance even with a thick P3CT-Na layer. The PCE could be stabilized over 11% even if the thickness of the P3CT-Na layer ranged from 1 nm to 52 nm, and the inferior PCE of p-PSCs with the thick P3CT-Na layer was mainly due to the decreased J_{sc} caused by the absorbance of P3CT-Na. Our work indicated that water soluble polyelectrolytes could also work well as an innovative type of HTM in perovskite solar cells. For further studies, the optimization of the chemical structure of P3CT-Na and alleviating the absorbance of the HTM layer could be an effective method to improve the device performance.

Acknowledgements

The project was supported by the National Natural Science Foundation of China (51273208, 61474125), Zhejiang Provincial Natural Science Foundation of China (LR14E030002) and the Ningbo Science and Technology Bureau (2014B82010). The work was also supported by the Hundred Talent Program of Chinese Academy of Sciences. We also acknowledge the support of Jiangsu Collaborative Innovation Center of Photovoltaic Science and Engineering (Changzhou, 213164, P.R China).

Notes and references

1 S. Kazim, M. K. Nazeeruddin, M. Grätzel and S. Ahmad, *Angew. Chem., Int. Ed.*, 2014, **53**, 2812–2824.
2 N.-G. Park, *J. Phys. Chem. Lett.*, 2013, **4**, 2423–2429.
3 H. J. Snaith, *J. Phys. Chem. Lett.*, 2013, **4**, 3623–3630.
4 L. Etgar, P. Gao, Z. Xue, Q. Peng, A. K. Chandiran, B. Liu, M. K. Nazeeruddin and M. Grätzel, *J. Am. Chem. Soc.*, 2012, **134**, 17396–17399.
5 S. D. Stranks, G. E. Eperon, G. Grancini, C. Menelaou, M. J. P. Alcocer, T. Leijtens, L. M. Herz, A. Petrozza and H. J. Snaith, *Science*, 2013, **342**, 341–344.
6 G. Xing, N. Mathews, S. Sun, S. S. Lim, Y. M. Lam, M. Grätzel, S. Mhaisalkar and T. C. Sum, *Science*, 2013, **342**, 344–347.
7 A. Kojima, K. Teshima, Y. Shirai and T. Miyasaka, *J. Am. Chem. Soc.*, 2009, **131**, 6050–6051.
8 H. Zhou, Q. Chen, G. Li, S. Luo, T.-b. Song, H.-S. Duan, Z. Hong, J. You, Y. Liu and Y. Yang, *Science*, 2014, **345**, 542–546.
9 J. Burschka, N. Pellet, S.-J. Moon, R. Humphry-Baker, P. Gao, M. K. Nazeeruddin and M. Gratzel, *Nature*, 2013, **499**, 316–319.
10 S. Ryu, J. H. Noh, N. J. Jeon, Y. C. Kim, W. S. Yang, J. W. Seo and S. I. Seok, *Energy Environ. Sci.*, 2014, **7**, 2614–2618.
11 M. M. Lee, J. Teuscher, T. Miyasaka, T. N. Murakami and H. J. Snaith, *Science*, 2012, **338**, 643–647.
12 A. Mei, X. Li, L. Liu, Z. Ku, T. Liu, Y. Rong, M. Xu, M. Hu, J. Chen, Y. Yang, M. Grätzel and H. Han, *Science*, 2014, **345**, 295–298.
13 N. J. Jeon, J. H. Noh, Y. C. Kim, W. S. Yang, S. Ryu and S. I. Seok, *Nat. Mater.*, 2014, **13**, 897–903.
14 K. Yan, M. Long, T. Zhang, Z. Wei, H. Chen, S. Yang and J. Xu, *J. Am. Chem. Soc.*, 2015, **137**, 4460–4468.
15 F. Wang, H. Yu, H. Xu and N. Zhao, *Adv. Funct. Mater.*, 2015, **25**, 1120–1126.
16 N. J. Jeon, J. H. Noh, W. S. Yang, Y. C. Kim, S. Ryu, J. Seo and S. I. Seok, *Nature*, 2015, **517**, 476–480.
17 G. E. Eperon, V. M. Burlakov, P. Docampo, A. Goriely and H. J. Snaith, *Adv. Funct. Mater.*, 2014, **24**, 151–157.
18 Q. Chen, H. Zhou, Z. Hong, S. Luo, H.-S. Duan, H.-H. Wang, Y. Liu, G. Li and Y. Yang, *J. Am. Chem. Soc.*, 2013, **136**, 622–625.
19 M. Liu, M. B. Johnston and H. J. Snaith, *Nature*, 2013, **501**, 395–398.
20 J.-Y. Jeng, Y.-F. Chiang, M.-H. Lee, S.-R. Peng, T.-F. Guo, P. Chen and T.-C. Wen, *Adv. Mater.*, 2013, **25**, 3727–3732.
21 P. Docampo, J. M. Ball, M. Darwich, G. E. Eperon and H. J. Snaith, *Nat. Commun.*, 2013, **4**, 2761.
22 J. Seo, S. Park, Y. Chan Kim, N. J. Jeon, J. H. Noh, S. C. Yoon and S. I. Seok, *Energy Environ. Sci.*, 2014, **7**, 2642–2646.
23 F. Zuo, S. T. Williams, P.-W. Liang, C.-C. Chueh, C.-Y. Liao and A. K. Y. Jen, *Adv. Mater.*, 2014, **26**, 6454–6460.
24 W. Nie, H. Tsai, R. Asadpour, J.-C. Blancon, A. J. Neukirch, G. Gupta, J. J. Crochet, M. Chhowalla, S. Tretiak, M. A. Alam, H.-L. Wang and A. D. Mohite, *Science*, 2015, **347**, 522–525.
25 J. You, Z. Hong, Y. Yang, Q. Chen, M. Cai, T.-B. Song, C.-C. Chen, S. Lu, Y. Liu, H. Zhou and Y. Yang, *ACS Nano*, 2014, **8**, 1674–1680.
26 J. You, Y. Yang, Z. Hong, T.-B. Song, L. Meng, Y. Liu, C. Jiang, H. Zhou, W.-H. Chang, G. Li and Y. Yang, *Appl. Phys. Lett.*, 2014, **105**, 183902.

27 O. Malinkiewicz, A. Yella, Y. H. Lee, G. M. Espallargas, M. Graetzel, M. K. Nazeeruddin and H. J. Bolink, *Nat. Photonics*, 2014, **8**, 128–132.

28 Z. Xiao, Q. Dong, C. Bi, Y. Shao, Y. Yuan and J. Huang, *Adv. Mater.*, 2014, **26**, 6503–6509.

29 W. Yongzhen, A. Islam, X. Yang, C. Qin, J. Liu, K. Zhang, W. Peng and L. Han, *Energy Environ. Sci.*, 2014, **7**, 2934–2938.

30 Z. Xiao, C. Bi, Y. Shao, Q. Dong, Q. Wang, Y. Yuan, C. Wang, Y. Gao and J. Huang, *Energy Environ. Sci.*, 2014, **7**, 2619–2623.

31 M. Kemerink, S. Timpanaro, M. M. de Kok, E. A. Meulenkamp and F. J. Touwslager, *J. Phys. Chem. B*, 2004, **108**, 18820–18825.

32 A. M. Nardes, M. Kemerink, R. A. J. Janssen, J. A. M. Bastiaansen, N. M. M. Kiggen, B. M. W. Langeveld, A. J. J. M. van Breemen and M. M. de Kok, *Adv. Mater.*, 2007, **19**, 1196–1200.

33 K.-G. Lim, H.-B. Kim, J. Jeong, H. Kim, J. Y. Kim and T.-W. Lee, *Adv. Mater.*, 2014, **26**, 6461–6466.

34 J.-Y. Jeng, K.-C. Chen, T.-Y. Chiang, P.-Y. Lin, T.-D. Tsai, Y.-C. Chang, T.-F. Guo, P. Chen, T.-C. Wen and Y.-J. Hsu, *Adv. Mater.*, 2014, **26**, 4107–4113.

35 J. H. Kim, P.-W. Liang, S. T. Williams, N. Cho, C.-C. Chueh, M. S. Glaz, D. S. Ginger and A. K. Y. Jen, *Adv. Mater.*, 2015, **27**, 695–701.

36 Z. Zhu, Y. Bai, T. Zhang, Z. Liu, X. Long, Z. Wei, Z. Wang, L. Zhang, J. Wang, F. Yan and S. Yang, *Angew. Chem.*, 2014, **126**, 12779–12783.

37 Z. Wu, S. Bai, J. Xiang, Z. Yuan, Y. Yang, W. Cui, X. Gao, Z. Liu, Y. Jin and B. Sun, *Nanoscale*, 2014, **6**, 10505–10510.

38 J. Morgado, R. H. Friend and F. Cacialli, *Appl. Phys. Lett.*, 2002, **80**, 2436–2438.

39 H. Yan, P. Lee, N. R. Armstrong, A. Graham, G. A. Evmenenko, P. Dutta and T. J. Marks, *J. Am. Chem. Soc.*, 2005, **127**, 3172–3183.

40 O. Malinkiewicz, A. Yella, Y. H. Lee, G. M. Espallargas, M. Graetzel, M. K. Nazeeruddin and H. J. Bolink, *Nat. Photonics*, 2013, **8**, 128–132.

41 O. Malinkiewicz, C. Roldán-Carmona, A. Soriano, E. Bandiello, L. Camacho, M. K. Nazeeruddin and H. J. Bolink, *Adv. Energy Mater.*, 2014, **4**, 1400345.

42 J. Shi, J. Dong, S. Lv, Y. Xu, L. Zhu, J. Xiao, X. Xu, H. Wu, D. Li, Y. Luo and Q. Meng, *Appl. Phys. Lett.*, 2014, **104**, 063901.

43 S. S. Hegedus and W. N. Shafarman, *Progress in Photovoltaics: Research and Applications*, 2004, **12**, 155–176.

44 X. Li, X. Wang, W. Zhang, Y. Wu, F. Gao and J. Fang, *Org. Electron.*, 2015, **18**, 107–112.

45 H. J. Snaith, A. Abate, J. M. Ball, G. E. Eperon, T. Leijtens, N. K. Noel, S. D. Stranks, J. T.-W. Wang, K. Wojciechowski and W. Zhang, *J. Phys. Chem. Lett.*, 2014, **5**, 1511–1515.

46 Z. Xiao, Y. Yuan, Y. Shao, Q. Wang, Q. Dong, C. Bi, P. Sharma, A. Gruverman and J. Huang, *Nat. Mater.*, 2015, **14**, 193–198.

47 E. L. Unger, E. T. Hoke, C. D. Bailie, W. H. Nguyen, A. R. Bowring, T. Heumuller, M. G. Christoforo and M. D. McGehee, *Energy Environ. Sci.*, 2014, **7**, 3690–3698.

48 W. Tress, N. Marinova, T. Moehl, S. M. Zakeeruddin, M. K. Nazeeruddin and M. Gratzel, *Energy Environ. Sci.*, 2015, **8**, 995–1004.

49 Q. Wang, Y. Shao, Q. Dong, Z. Xiao, Y. Yuan and J. Huang, *Energy Environ. Sci.*, 2014, **7**, 2359–2365.

50 T. Leijtens, S. D. Stranks, G. E. Eperon, R. Lindblad, E. M. J. Johansson, I. J. McPherson, H. Rensmo, J. M. Ball, M. M. Lee and H. J. Snaith, *ACS Nano*, 2014, **8**, 7147–7155.

51 L. Zuo, Z. Gu, T. Ye, W. Fu, G. Wu, H. Li and H. Chen, *J. Am. Chem. Soc.*, 2015, **137**, 2674–2679.

52 S. Pathak, A. Sepe, A. Sadhanala, F. Deschler, A. Haghighirad, N. Sakai, K. C. Goedel, S. D. Stranks, N. Noel, M. Price, S. Hüttner, N. A. Hawkins, R. H. Friend, U. Steiner and H. J. Snaith, *ACS Nano*, 2015, **9**, 2311–2320.

53 J.-H. Im, J. Luo, M. Franckevičius, N. Pellet, P. Gao, T. Moehl, S. M. Zakeeruddin, M. K. Nazeeruddin, M. Grätzel and N.-G. Park, *Nano Lett.*, 2015, **15**, 2120–2126.

54 Z. He, C. Zhong, S. Su, M. Xu, H. Wu and Y. Cao, *Nat. Photonics*, 2012, **6**, 591–595.

55 Y. Zhou, C. Fuentes-Hernandez, J. Shim, J. Meyer, A. J. Giordano, H. Li, P. Winget, T. Papadopoulos, H. Cheun, J. Kim, M. Fenoll, A. Dindar, W. Haske, E. Najafabadi, T. M. Khan, H. Sojoudi, S. Barlow, S. Graham, J.-L. Brédas, S. R. Marder, A. Kahn and B. Kippelen, *Science*, 2012, **336**, 327–332.